analytical chemistry

pubs.acs.org/ac Article

Developing a Paper-Based Antigen Assay to Differentiate between Coronaviruses and SARS-CoV-2 Spike Variants

Delyan Hristov, Hom Rijal, Jose Gomez-Marquez, and Kimberly Hamad-Schifferli*

Cite This: *Anal. Chem.* 2021, 93, 7825−7832 Read Online

ACCESS | Metrics & More | Article Recommendations | Supporting Information

ABSTRACT: COVID-19 first appeared in December of 2019 in Wuhan, China. Since then, it has become a global pandemic. A robust and scalable diagnostics strategy is crucial for containing and monitoring the pandemic. RT-PCR is a known, reliable method for COVID-19 diagnostics, which can differentiate between SARS-CoV-2 and other viruses. However, PCR is location-dependent, time-consuming, and relatively expensive. Thus, there is a need for a more flexible method, which may be produced in an off-the-shelf format and distributed more widely. Paper-based immunoassays can fulfill this function. Here, we present the first steps toward a paper-based test, which can differentiate between different spike proteins of various coronaviruses, SARS-CoV-1, SARS-CoV-2, and CoV-HKU1, with negligible cross-reactivity for HCoV-OC43 and HCoV-229E in a single assay, which takes less than 30 min. Furthermore, our test can distinguish between fractions of the same spike protein. This is done by an altered assay design with four test line locations where each antigen builds a unique, identifiable binding pattern. The effect of several factors, such as running media, immunoprobe concentration, and antigen interference, is considered. We find that running media has a significant effect on the final binding pattern where human saliva provides results while human serum leads to the lowest signal quality.

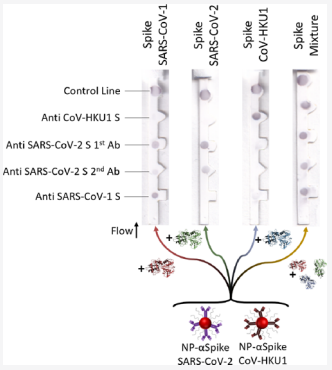

INTRODUCTION

The COVID-19 global pandemic, which emerged in Wuhan, China in December of 2019, has infected millions of people and caused or contributed to the death of hundreds of thousands and led to an economic downturn. Diagnosis of COVID-19 using diagnostic tools is preferable over clinical symptoms due to the nonspecific nature of COVID-19 symptomology. The majority of patients suffer non-specific, mild symptoms mostly consisting of cough, fever, muscle pain, and nausea.[1,2] Additionally, an estimated 20−80% of patients are asymptomatic, with varying reports.[3−5] Traditional laboratory diagnostics such as RT-PCR have high sensitivity and diagnostic accuracy but are expensive and time-consuming and may not be locally available. Paper-based immunoassays can compliment PCR and contribute to a better diagnostics strategy. While they commonly suffer from relatively low selectivity and especially sensitivity, compared to PCR, paper-based tests are cheap to produce locally or in an at-scale manufacturing facility and can be made in an off-the-shelf format and stored for prolonged periods of time in mild conditions, *e.g.*, room temperature or 4 °C.[6] Furthermore, their flexible design allow simultaneous detection of multiple targets.[7,8]

Paper-based tests for SARS-CoV-2 detection can be classified as antibody (or serological) tests, *i.e.*, those that measure the host immune response, and antigen tests, *i.e.*, those that bind to viral antigens.[9] Antigen paper-based immunoassays typically target the spike (S) or nucleocapsid (N) proteins. The S protein decorates the outside of coronaviruses and enables their uptake into cells.[10] Variances in the S protein structure determine the cellular uptake pathway and affinity of the virus for the cell. SARS-CoV-2, similar to SARS-CoV-1 and HCoV-NL63, targets the ACE2 receptor in the oral and nasal cavities as its primary root of infection.[11,12] The S protein has been shown to be a primary driver of viral evolution, where mutations greatly impact the virus infection rate and is considered to be the primary difference in reproductive number between clades.[13,14]

A low-cost, rapid, and user-friendly platform that can differentiate is desirable. Distinguishing between respiratory viruses with similar clinical symptoms is especially important not only to provide timely treatment but also to better assess patient risk. Here, we present the first step toward developing a paper-based sensor, which can differentiate between S proteins from different coronaviruses as well as spike protein variants from SARS-CoV-2. The test relies on a sandwich immunoassay and antibody cross-reactivity for antigen specific test patterns. We used a set of six commercially available antibodies and seven commercially available S proteins to establish strategy viability. The test was able to differentiate between all antigens,

Received: December 28, 2020
Accepted: May 14, 2021
Published: May 26, 2021

https://doi.org/10.1021/acs.analchem.0c05438
Anal. Chem. 2021, 93, 7825−7832

including SARS-CoV-2 spike fragments. Test limit of detection (LOD) was in the 0.1 nM range, which may be sufficient for viral detection in more severe cases. We also studied the effect of running medium on test efficacy, bovine serum albumin (BSA), human serum (HS), and saliva.[15]

MATERIALS AND METHODS

Gold NP Synthesis. Milli-Q water (47.2 g) was weighed into a glass bottle. A 10 mg/mL solution of $HAuCl_4$ (1.4 mL, Sigma) was pipetted in after which the bottle was placed in a water bath resting on a reaction station and stirred. The water in the bath was brought to a boil and left to fully equilibrate for >15 min. The lid was carefully removed, and 0.9 mL of 10 mg/mL sodium citrate (tribasic sodium citrate, Sigma) was added under vigorous stirring. The lid was replaced, and the solution was left to react for ∼15 min. During this time, the solution changed color from pale yellow to almost black to wine red as NPs formed. Final concentrations of $HAuCl_4$ and sodium citrate were 0.83 and 0.62 mM, respectively.

Immunoprobe Synthesis. Immunoprobe synthesis followed our previous work.[16] An appropriate amount of as-synthesized NPs was pipetted into a LoBind Eppendorf (Sigma). A 1 mg/mL solution (6.5 μM) of the antibody (10 μL) (Table S2) was added per mL of AuNPs for a final antibody concentration of 0.065 μM. The solution was left to shake gently at room temperature (RT) for an hour. Then, 10 μL of 1 mg/mL (0.2 mM) MeO-PEG_{5000}-SH (NanoCS) was added for a final concentration of 0.002 μM. The dispersion was left to react for 1 h. Particles were washed 2× with PBS via centrifugation (8000 rpm for 10 min). The dispersion was resuspended in 1/20th of the initial volume. Vortexing and brief sonication (up to 3 s at a time) were used to disperse the particles when needed. The immunoprobes were stored at 4 °C for up to 3 weeks.

UV−Vis Spectroscopy. Immunoprobes (2 μL) were diluted in 198 μL of PBS in a 96-well plate. A SpectraMax M5 (Molecular Devices) plate reader measured spectra 400−800 nm at 1 nm intervals.

DLS. Dispersions were taken from the UV−Vis plate as is and placed into a 1.5 mL plastic cuvette (Sigma). PBS (100 μL) was added (total volume of 300 μL). Each dynamic light scattering (DLS) (Horiba SZ-100) measurement was the result of five runs on automatic and at 25 °C. The running medium was always specified as water and the particle material as gold (n = 0.2−3.32i).

Dipstick Preparation. Nitrocellulose strips were cut with a laser cutter and assembled into dipstick assay strips as needed. The as-made dipsticks were stained with 0.3 μL of 1 mg/mL of the target antibody (Table S2) at the test line and α-Rabbit Fc at the control line. All staining was done on the day of use. Dipsticks were left to dry for >10 min at RT prior to immersion in the sample. For direct antigen binding dipsticks, 0.3 μL of the pure antigen was pipetted on the test line instead of an antibody.

Running Dipsticks. Target antigen was added to the sample and diluted via serial dilution in titration experiments. In a typical non-titration experiment, 1 μL of antigen solution at 10^{-2} mg/mL was added to 30 μL of the running medium and homogenized. For titrations, 1 μL of a 1 mg/mL antigen solution was added to 39 μL of the running medium. A serial dilution was done as 10 μL of the as-made solution was added in a tube containing 30 μL of the running medium and homogenized, and the process was repeated up to nine times for a total of 10 samples (nine with reducing antigen concentration and one control). The final 10 μL was discarded. The negative control contained 30 μL of the running medium.

Single immunoprobes (2 μL, 6.25% v/v) or immunoprobe mixtures (4 μL, 11.8% V/V) were pipetted to antigen solutions, homogenized, and left at RT for 10−30 min. Then, 15 μL of running buffer (1:1 volumetric mixture of 50% sucrose and 1% Tween) was added. The dispersion was spun in a mini centrifuge (∼1.5 krpm), vortexed, and left for 5−15 min. Dipsticks were immersed into the dispersion and left to run. After the full sample volume diffused through the paper, 1% Tween80 was added to remove non-specifically bound particles. Strips were left overnight at RT to dry.

Immunoprobe Volume Experiment for Altered Dipstick Design. For the altered dipstick design, the volume of immunoprobes was varied while keeping the sample volume constant (SI Figure S9). Immunoprobes (either individual or mixture) (1, 2, 4, 6, and 8 μL) were placed in 30 μL of the sample with an antigen concentration of 1×10^{-3} mg/mL.

Image Analysis. Dried dipsticks were affixed to white paper and scanned. The nitrocellulose area was analyzed in ImageJ.[17] The mean gray value of the measurement tool was used to obtain grayscale values. The area of the rectangle used was fixed to be within the particle signal and kept constant for each image analysis. Shadows and edges were avoided as they introduced artifacts. The background grayscale value was evaluated by measuring a visibly "empty" area near the test and control lines. For three location strips, this was the bottom square location. For five location strips, each strip had a separate background measurement located just below or above the test area. Antigen titrations were fit with a single Langmuir curve by an in-house written Python script to obtain K_D^{Eff} and A values (SI Calculations section).

LOD Analysis. Test LOD was calculated from the Langmuir fits of the antigen titration curves according to equations in the Supporting Information.

Distribution Analysis. Images were analyzed following our previous work[16] using the gel analysis tool in ImageJ.[17] The signal integration obtained from the analysis was converted to fractions in Microsoft Excel.

Heatmap and Pattern Generation. Grayscales obtained via ImageJ were averaged by condition, immunoprobe, and running medium and normalized as a percent of the highest value. Grayscales were binned at 0−20%, 21−40%, 41−60%, 61−80%, and 81−100% where each, except the lowest category, was assigned a darker shade of green.

RESULTS

Immunoprobe Screening. We chose spike protein as a target because it protrudes from the viral particle and is responsible for receptor recognition. It is composed of the S1 and S2 parts, where the receptor binding domain (RBD) is in S1.[18] We obtained S1 proteins for SARS-CoV-2, SARS-CoV-1 (SARS), and non-lethal coronaviruses CoV-HKU1 (HKU1), HCoV-OC43 (OC43), and HCoV-229E (229E) to study the selectivity of our nanoparticle-antibody conjugates (NP-Ab conjugates or immunoprobes). SARS-CoV-2 was termed COVID (Table 1 and Table S1).

All antibodies used were commercially available. Six antibodies were evaluated for antigen binding and sandwich immunoassay formation (Table 1 and Table S2). Two were raised against SARS-CoV-2 (αC1-2), three for SARS (αS1-3), and one for CoV-HKU1 (αH). Gold NP-Ab conjugates were

https://doi.org/10.1021/acs.analchem.0c05438
Anal. Chem. 2021, 93, 7825−7832

Table 1. Antigens, Antibodies, and NP-Ab Conjugates Used

antigens		antibodies		
antigen	virus	antibody	NP-Ab	virus
COVID 1	SARS-CoV-2	αC1	NP-αC1	SARS-CoV-2
COVID 2	SARS-CoV-2	αC2	NP-αC2	SARS-CoV-2
COVID 3	SARS-CoV-2	αS1	NP-αS1	SARS-CoV-1
SARS	SARS-CoV-1	αS2	NP-αS2	SARS-CoV-1
229E	HCoV-229E	αS3	NP-αS3	SARS-CoV-1
OC43	HCoV-OC43	αH	NP-αH	CoV-HKU1
HKU1	CoV-HKU1			

synthesized using literature methods.[16,19] Briefly, each antibody was conjugated to the NPs by physisorption, and then thiolated PEG was added after conjugation to backfill open areas on the NP surface. Dynamic light scattering (DLS) and UV−Vis spectroscopy were used to determine colloidal stability and size dispersion in PBS. DLS of NPs in BSA, saliva, and HS obtained hydrodynamic diameters (D_H) of ∼65 nm, which increased ∼85 nm after antibody conjugation, supporting conjugation (SI Figures S1 and S2). D_H increased further to 120−200 nm in media, possibly due to protein adsorption to the NP surface.

Antibody target and off-target binding were studied using antigen and sandwich dipstick assays. In the former case the antigens were immobilized on nitrocellulose following which the prepped strips were immersed in an immunoprobe dispersion (Figure 1a). For sandwich immunoassays, antigen binding to the immobilized antibody and also the immunoprobe was tested (Figure 1c). α-rabbit IgG Fc (α-Fc), was immobilized at the control area during both tests. A signal at the test line certified that the fluid flowed through the paper strip. Localized signal emerges on the strip due to immunoprobe accumulation (Figure 1a,c). NP-αS2 and NP-αS3 NPs were eliminated due to poor performance in initial tests (SI Figure S3).

After running, strips were left to dry overnight at room temperature after which they were scanned and analyzed *via* ImageJ.[17] The resulting grayscale values were normalized to 100% and plotted as a heatmap for clarity (Figure 1b), where white represents low intensity (<20% of maximum value) and green high. Averaged grayscale values are provided in the Supporting Information.

In antigen binding tests, NP-αC1 and NP-αC2 bound to both COVID and SARS antigens, but not other coronavirus antigens. NP-αS1 bound to its target antigen, SARS, and exhibited some cross-reactivity for COVID 1 and OC43. Immunoprobe binding in saliva resulted in similar signal intensities but were notably lower in human serum (HS) (Figure 1b and Figures S4 and S5), which could be attributed to HS screening of the immunoprobe function.[9]

We evaluated the ability of the immunoprobes to form a sandwich immunoassay in a dipstick (Figure 1c).[20] Sandwich formation relies on two reactions, immunoprobe-antigen and printed antibody-antigen binding. The choice of both antibodies is primary during test design, where antibody pairs (on the immunoprobe/printed on the paper) with varying affinity and selectivity for a target can be used to detect a wider variety of antigens and develop a binding pattern.[21] In this initial study, we screened the pairing of an antibody with itself, *i.e.*, NP-αS1 run with immobilized αS1 (NP-αS1/αS1), NP-αC1 with αC1 (NP-αC1/αC1), NP-αC2 with αC1 (NP-αC2/αC1), and NP-αH with αH (NP-αH/αH). αC2, a monoclonal antibody, did not form a sandwich with itself.

NP-αC1/αC1 and NP-αC2/αC1 were able to successfully form sandwich immunoassays with both COVID and SARS antigens, as indicated by the color resulting at the test line (Figure 1d and SI Figures S6 and S7). NP-αS1/αS1 could detect the SARS antigen, but not COVID antigens. The

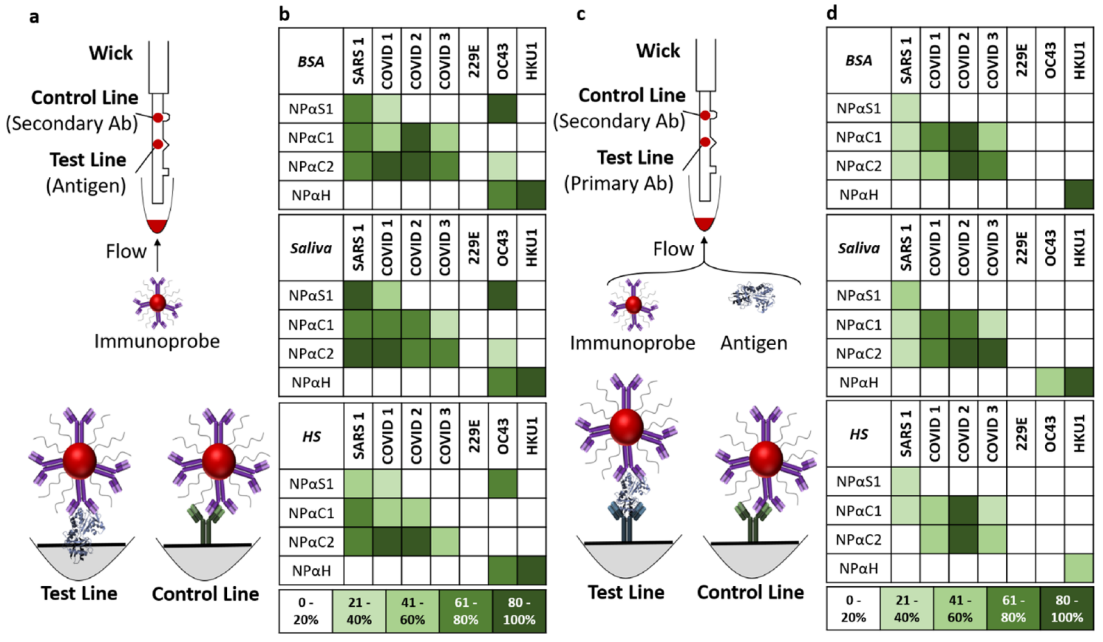

Figure 1. Antibody screening. (a) Experimental setup for direct antigen binding tests and (b) average test area intensities run in triplicate in BSA, saliva, and HS. (c) Experimental setup for sandwich immunoassays and (d) average test area intensities in BSA, saliva, and HS. Intensities were of all strips were normalized. Averaged results are from at least three independent batches. Related grayscale values and standard deviations are shown in SI Figures S5 and S7.

https://doi.org/10.1021/acs.analchem.0c05438
Anal. Chem. 2021, 93, 7825−7832

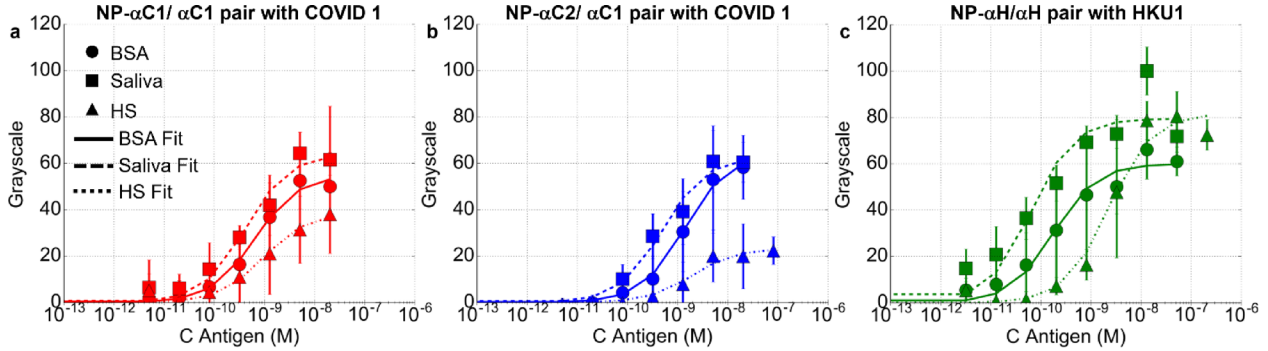

Figure 2. Immunoprobe performance. Titration curves of selected pairs. (a) NP-αC1/αC1 run with COVID 1, (b) NP-αC2/αC1 run with COVID 1, and (c) NP-αH1/αH1 run with HKU1.

observed difference in behavior is potentially due to protein folding. NP-αC1/αC1 and NP-αC2/αC1 exhibited no cross-reactivity for 229E, OC43, and HKU1, and NP-αH/αH exhibited a signal only with HKU1.

Pairs were also tested in saliva and HS (Figure 1d), and the behavior was largely similar to BSA except for NP-αH/αH exhibiting some cross-reactivity toward OC43 in saliva. Saliva resulted in similar intensities to BSA, but intensities were significantly lower in HS, highlighting the importance of the biological media. Generally, direct antigen binding had a higher signal and cross-reactivity than sandwich formation (Figure 1b,d).

Cross-reactivity was more commonly observed in saliva compared to the other media. This could be attributed to slower flow due to surface tension,[22] which results in a longer residence time of the immunoprobe-antigen complex near the test areas and increases binding probability. A compounding factor could be saliva composition, which has different surfactants or macromolecules and a lower pH (6−7)[23,24] compared to BSA and HS (7.4). We expect the low protein concentration of saliva to be a major factor, which is >99% water (wt/wt) and ∼1 mg/mL protein[22] compared to BSA (30 mg/mL) and HS (60−80 mg/mL). Test backgrounds in all three media were similar, suggesting low non- specific binding of the immunoprobes to the paper.

Antigen cross-reactivity could be attributed to proximity in phylogeny. Cross-reactivity between SARS and SARS-CoV-2 antibodies and antigens was expected due to ∼82% sequence similarities,[13,25,26] while the proximity between the RBD regions is ∼73%.[13] NP-αH bound to its target antigen HKU1, as well as OC43 presumably due to proximity in phylogeny.[10] Antigen sequences were compared to each other and the Wuhan reference strain structure (accession number YP_009724390.1) using MUSCLE (SI Figure S8a). Structural differences in MUSCLE can arise from both sequence length and content; therefore, it is expected that some structural dissimilarities arise our antigens being recombinant fractions of the S protein. HKU1 had the highest structural similarity with the Wuhan reference strain (20%) and lowest with COVID 1 (10%). SARS had an ∼50% structural similarity with COVID 1 and 2 and ∼28% with COVID 3 and the Wuhan strain. Similarity between the COVID antigens and compared with the Wuhan strain were 30−50%. Comparison of the RBD of all COVID antigens revealed a 100% structural similarity (SI Figure S8b). COVID 1 had a 98% similarity with the Wuhan strain (SI Figure S8c).

Quantifying Sandwich Immunoassay Performance in Different Media. Sandwich immunoassay performance was investigated by quantifying their limit of detection (LOD) and effective dissociation constant (K_D^{Eff}) for their target antigens. NP-αC1/αC1, NP-αC2/αC1, and NP-αH/αH were titrated with COVID 1 and HKU1 antigens in BSA, HS, and saliva. Test line intensities were measured and fit with a modified Langmuir equation[16,19,27] to obtain K_D^{Eff}. LOD was calculated separately, defined as the background signal + 3 × the standard deviation of the background (SI Calculations section). LODs ranged from 0.1 to 0.17 nM, while K_D^{Eff} values were in the 10^{-10} M range (Figure 2a−c, Table 1, and Table S3).

Changing the running media impacted the performance. Compared to BSA, antibody pairs generally performed similarly or better in saliva and worse in HS (Figure 2a−c and Table 1). The LOD of NP-αC1/αC1 was the lowest in BSA and 2× higher in saliva and 7× in HS (Figure 2a and Table 1). Titration curves of NP-αC2/αC1 were the lowest in BSA, followed by saliva (3×), and significantly higher in HS (9×) (Figure 2b).

Between the two SARS-CoV-2 pairs, NP-αC1/αC1 exhibited a comparable behavior but marginally outperformed NP-αC2/αC1 in all media by ∼2×. This is consistent with sandwich results where NP-αC1/αC1 had a higher intensity with COVID 1 than NP-αC2/αC1. The NP-αH/αH behavior changed the most with running media, where LOD and K_D^{Eff} values varied by two orders of magnitude between saliva and HS. LODs were 0.07 nM in saliva and 0.54 nM in HS. K_D^{Eff} values were 0.06 nM in saliva and 2.78 nM in HS (Table 2 and Figure 2c).

Control of Antigen Detection through Cross-Reactivity. We then investigated how the test could be used as a multiplexed assay to differentiate between SARS-CoV-2 antigens with a similar structure and other coronavirus species, building on the ability to strategically use cross-reactive

Table 2. LOD and K_D^{Eff} Values of Pairs for Target Antigens in BSA, Saliva, and HS

	BSA		saliva		HS	
	LOD (nM)	K_D^{Eff} (nM)	LOD (nM)	K_D^{Eff} (nM)	LOD (nM)	K_D^{Eff} (nM)
NP-αC1/αC1 with COVID 1	0.08	0.41	0.24	0.26	0.59	0.6
NP-αC2/αC1 with COVID 1	0.17	0.88	0.56	0.32	1.56	1.28
NP-αH/αH with HKU1	0.03	0.18	0.07	0.06	0.54	2.78

https://doi.org/10.1021/acs.analchem.0c05438
Anal. Chem. 2021, 93, 7825−7832

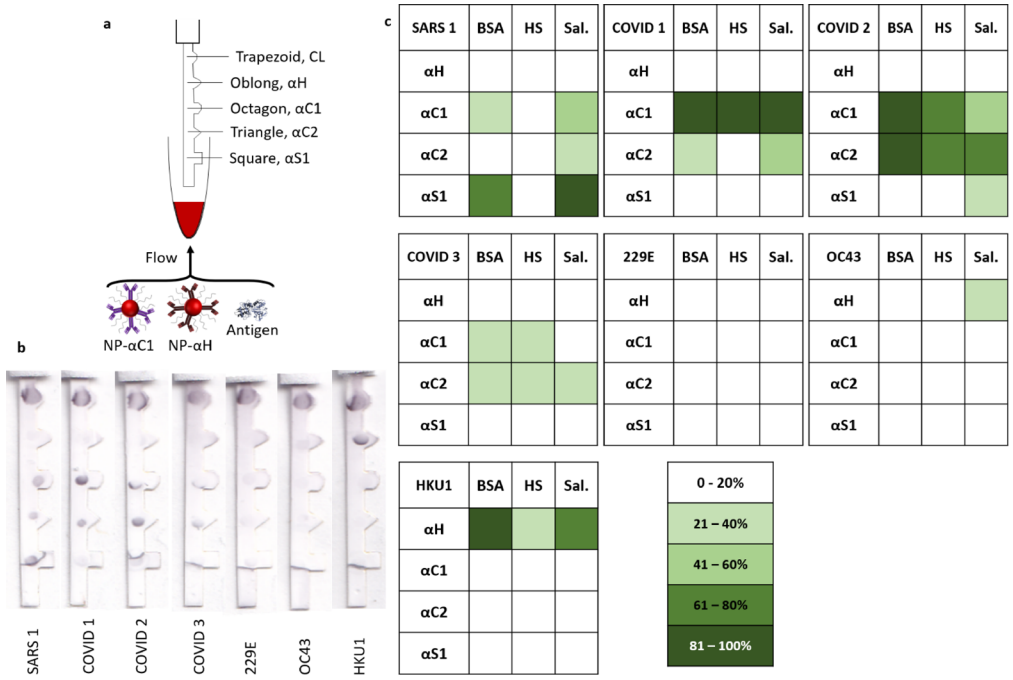

Figure 3. Altered strip design and antigen binding patterns. (a) Schematic of experimental procedure, b) example strips run in saliva, and (c) average test area intensities run in triplicate in BSA, saliva, and HS. Intensities of all strips were normalized. Grayscale values for test are shown in SI Figure S11.

antibodies to differentiate between different antigens.[21] We first studied the relevance of both binding events on sandwich formation and antigen detection. The signal of combinations of all three antigens (SARS, COVID 1, and HKU1), immunoprobes (NP-αC1, NP-αC2, and NP-αH), and printed antibodies (αS1, αC1, and αH) was measured (total of 27 combinations, Figure S9a). Experiments were repeated in triplicate in BSA at antigen concentrations of 1×10^{-3} mg/mL.

SARS was detectable only with the NP-αC1/αS1 and NP-αC2/αS1 pairs. COVID 1 was detectable only with the NP-αC1/αC1 and NP-αC2/αC1 pairs, and HKU1 was detectable only with the NP-αH/αH pair (SI Figure S9b,c). This further confirmed that HKU1 was not cross-reactive with the other coronavirus antibodies.

These results reaffirm the efficacy of the cross-reactivity strategy, where only SARS was detected at immobilized αS1 and only COVID 1 at immobilized αC1. We attribute this to the lower affinity of cross-reactive interactions, which was confirmed by off-target antigen titrations (SI Figure S10). The NP-αC1/αC1 and NP-αS1/αC1 antibody couples were titrated with their off-target antigens, being SARS and COVID 1, respectively (SI Figure S10 and Tables S4 and S5). Both showed a reduced signal in all media compared to their on-target immunoprobe performance. There was no significant difference in LOD and K_D^{Eff} for NP-αC1/αC1 compared to its on-target COVID 1 titration (Tables S4 and S5).

Our results suggest that detection of SARS and COVID 1 is more dependent on the printed antibody rather than the one conjugated to the AuNPs. On average, there was an order of magnitude drop in off-target interactions, compared to on-target ones, *e.g.*, NP-αC1/αS1 to NP-αC1/αC1 with SARS (SI Figure S9b,c). These results indicate that cross-reactivity can be used for generating patterns.

Multiplexed Test. We designed multiplexed assay to differentiate between spike antigens of SARS and COVID 1, 2, and 3 and simultaneously detect spike from a non-lethal coronavirus, HKU1. The strip consisted of a control and four test areas at differently shaped locations (Figure 3a). Choice of location shape was to differentiate locations easier. Test area geometry did not have a measurable impact on signal quality. The antibodies immobilized at the test locations were (bottom to top) αS1, αC2, αC1, and αH. A 1:1 volumetric mixture of NP-αC1 and NP-αH was used to detect all antigens.

Running the assay with the different antigens produced characteristic binding patterns at the four test areas. SARS and COVID antigens were detectable on all locations except the αH area in saliva (Figure 3b). SARS resulted in signal mostly at the αS1 location, with lower signals at αC1 and αC2. COVID 1 exhibited the highest signal at αC2 and lower signal with αC1 and αS1 (Figure S3b). COVID 2 was only detectable at αC areas with comparable signal intensity at both locations (Figure 3b). As expected from its structure, COVID 3 produced signal mostly at the αC2 area. 229E and OC43 antigens in saliva yielded no significant signal, and HKU1 was observable only at the αH test area.

Again, signals were similar in BSA and saliva but were either reduced in intensity or lost in HS. For example, SARS could not be detected in HS but display a characteristic pattern in BSA and saliva (Figure 3c, top left). The HKU1 signal was the strongest in BSA and weakest in HS, which was consistent with single strip results (Figures 1d and 2c). Cross-reactivity was observed more often in saliva, where SARS was detectable at the αC2 location, COVID 2 was detectable at the αS1 location, and OC43 was detectable at αH.

Changing the format from singleplexed (Figure 1) to multiplexed modified the LOD slightly. We found that the LOD for COVID 2 increased from 0.054 nM in the singleplexed test to 0.21 nM in the multiplexed one (SI Figure

https://doi.org/10.1021/acs.analchem.0c05438
Anal. Chem. 2021, 93, 7825−7832

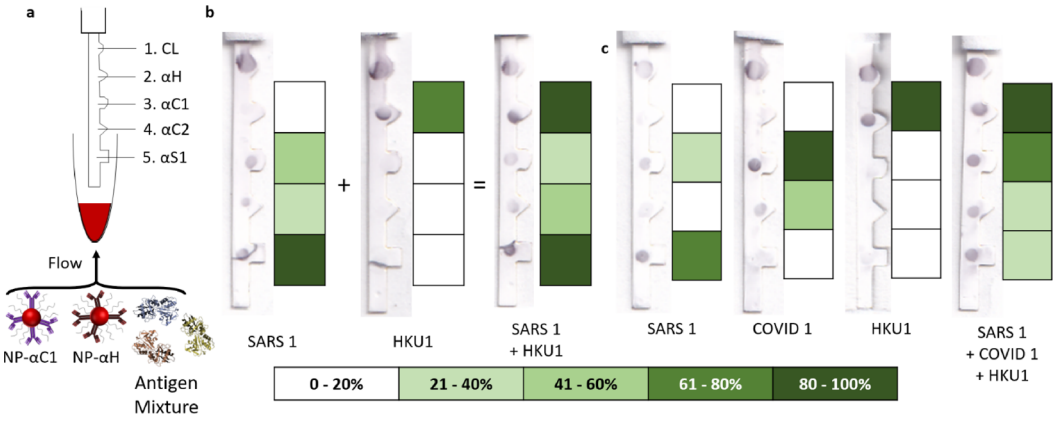

Figure 4. Running antigen mixtures in altered strip design. (a) Schematic of experimental procedure, (b) example strips, patterns, and from a test run with SARS 1 + HKU1 and (c) SARS1 + COVID 1 + HKU1.

S17). While this is a noticeable change, it is still not as dramatic as the LOD increase from changing the media to HS.

Interference between Multiple Antigens in the Multiplexed Test. We ran antigen mixtures to investigate binding interference (Figure 4a). When a mixture of SARS + HKU1 in BSA was run, an intensity appeared at all four test areas, with a higher intensity at αH and αS1. This pattern resembled the additive intensity pattern of SARS alone plus HKU1 alone (Figure 4b and SI Figure S13e,i,j). This suggested that the antigens did not compete with each other for forming immunoassay pairs. Results suggest that the binding pattern in the presence of multiple antigens is similar to mathematically adding the two independent patterns if the two antigens did not bind to the same immunoprobe, *e.g.*, SARS 1 and HKU1 (Figure 4b and SI Figures S13 and S14).

However, for antigens that bind to the same immunoprobe, the pattern depended on the affinity of the interaction. When a mixture of SARS1 + COVID 1 + HKU1 was run, an intensity appeared at all four test areas, showing that the test could simultaneously detect SARS, COVID1, and HKU1. However, the intensity pattern did not resemble what would be anticipated from simply adding the intensities of the individually run antigens (Figure 4c). Since SARS and COVID 1 interact with NP-αC1 with a similar dissociation constant (K_D^{Eff} (SARS) = 0.86 nM, K_D^{Eff} (COVID 1) = 0.42 nM), the pattern of the mixture depended on the relative concentration of the two antigens. In this case, the antigen with the higher concentration would have a more pronounced pattern (SI Figures S12, S13a,b,f, and S14a,b,f). Similar effects were observed for a SARS, COVID 1, and COVID 2 mixture (K_D^{Eff} (COVID 2) = 0.10 nM, SI Figure S12).

Some challenges arose with the multiplexed strip. Background gradients were more common in longer strips. To accommodate for this, we limited the strip to five test locations and modified the image analysis. We immobilized antibodies with a higher affinity further up the strip so they would not deplete the immunoprobe/antigen complexes before they encountered lower affinity immobilized antibodies. An optimal immunoprobe or immunoprobe mixture concentration was determined to be 12−17% of the total sample volume (SI Figure S15). By understanding and controlling these principles, it was possible to simultaneously detect and differentiate all three coronavirus antigens (Figure 4c and SI Figures S13 and S14).

DISCUSSION

The paper-based immunoassay investigated here was able to differentiate spike antigens from different coronaviruses by building a binding pattern through the number, arrangement, and specificity of printed antibodies. Differentiation between SARS-CoV-1, SARS-CoV-2, and HKU1 S1 proteins was simpler based on their patterns where SARS bound mostly to the NP-αC1/αS1 pair while HKU1 bound exclusively to NP-αH/αH. Negligible cross-reactivity with 229E and OC43 was observed.

The ability to differentiate between SARS-CoV-2 antigens is especially interesting and could yield new information for patient samples. We applied our test to three recombinant S1 fragments, COVID 1 with a length of 681 amino acids (aa), COVID 2 with 461 aa, and COVID 3 with 229. Considering the high sequence similarity (SI Figure S8), the difference in binding pattern can be attributed to their size. Thus, the use of binding patterns may be able to differentiate between different spike products in patient samples. This may help address some of the questions raised about patient viral shedding over time.[28] Differentiation between spike protein variants or fractions may be improved by increasing the specificity and number of antibodies printed on the nitrocellulose. It is unlikely that the assay would be able to differentiate between spike proteins from different clades due to the high sequence similarity (>99%).

The ability to detect and differentiate between antigen from other coronaviruses and antigen mixtures should not be overlooked. Co-circulation of non-lethal coronaviruses, other respiratory viruses, and SARS-CoV-2 has been reported.[29−31] Co-infections between SARS-CoV-2 with other respiratory viruses are rare, reported in 3−20% of cases, including co-infections with non-lethal coronaviruses in about 0.1−5% of cases.[32,33] However, a recent study suggests that co-infection of SARS-CoV-2 with influenza can increase the risk of poor patient outcomes.[29] Co-infection may also help explain reported abnormal viral shedding patterns and differences in patient outcomes, so a test that can simultaneously differentiate between common respiratory viruses would help address these questions.

The running media impacted antigen binding, where strips run in BSA and saliva had comparable results with a 15% variation in signal, lower than test-to-test variability. Running assays in HS resulted in a reduction or complete loss of signal, which could be attributed to protein screening effects.[16,34]

https://doi.org/10.1021/acs.analchem.0c05438
Anal. Chem. 2021, 93, 7825−7832

LODs for COVID antigens in BSA and saliva were in the ~ng/mL range (0.03−0.56 nM). In comparison, others have reported similar performance with a LOD of 0.62 ng/mL (0.0125 nM) for half strips for SARS-CoV-2 nucleocapsid (N) proteins.[20,35] We caveat that the LOD measurement was based on purified antigens in solution and not the full virus capsid in biological fluids, and matrix effects in patient samples or differences in spike secondary structure could influence the performance. We estimate the average number of spike proteins in sputum swabs to be in the pM range for most cases and nM range in more severe cases. This estimate is based on the average copies of RNA per mL of saliva[36] and assumes that every RNA copy corresponds to a virus, where each virus has 100 spike surface proteins,[37] and that there are no free spike proteins (SI Calculations section). While the concentration of spike protein in patient samples over time has still not been definitively quantified, it is anticipated that the LOD here may be too high for visual readouts for most patient samples.[37−40]

The intensity in a paper-based sandwich immunoassay depends on multiple factors, including antibody affinity, immunoprobe concentration, antibody coverage on the NP, NP size, and immobilized capture antibody concentration.[9] Varying these parameters can improve the signal intensity without external enhancement approaches. Commercial diagnostics have solved this with dedicated readers for colorimetric or fluorescent readouts (Sofia, Quidel Corp.). Surface enhanced Raman spectroscopy (SERS) nanotags,[41,42] isotachaphoresis,[43] and photothermal heating[44] have all been used successfully to increase the signal, sometimes as high as 100-fold. Simply running the flow back and forth over multiple passes can increase the signal 5-fold and does not require additional readout instrumentation.[7] Additionally, concentrating the antigen by sample preparation techniques or paper-fluidic design could increase the signal. Ultimately, this sensitivity gap could be solved by a combination of techniques.[45]

Test variability was estimated through the standard deviation and relative standard deviation (RSD) from all tests (SI Figure S16) to be 36%, which did not change significantly between media or antigen mixtures. Typically, lower signals and weaker antigen−antibody interactions resulted in higher RSDs. Variability is related to test robustness, which is an important factor for long-term storage. Prior studies have shown that the protein corona formed around the NP-Ab conjugate from the proteins in the patient sample can impact sandwich immunoassay formation with the target[27] and that the immunoassay performance is sensitive to NP aggregation.[16] Therefore, the sample matrix can impact the performance. BSA was used here as a test case in which the performance could be quantified and compared to a behavior in the running media of human saliva and serum, which were investigated as real biological media. Ultimately, the impact of environmental factors such as temperature and storage conditions on test robustness still needs to be explored, especially when considering for use in low-resource settings.[46]

Results presented here can be used toward the development of COVID-19 paper-based dipstick and lateral flow assays, a rapid diagnostic format that has aided in disease management, quarantine, and surveillance. The low production cost and relative ease of use of paper rapid diagnostics makes them suitable for both local and large-scale production, making it a potentially powerful off-the-shelf complement to RT-PCR, which could help elevate strain on local diagnostic facilities to meet the massive demand for tests. The self-contained nature of paper-based tests makes them attractive for remote or mobile locations.

■ ASSOCIATED CONTENT

Supporting Information

The Supporting Information is available free of charge at https://pubs.acs.org/doi/10.1021/acs.analchem.0c05438.

Secondary figures and tables providing the context for the text, calculations used, and methods section (PDF)

■ AUTHOR INFORMATION

Corresponding Author

Kimberly Hamad-Schifferli − *Department of Engineering and School for the Environment, University of Massachusetts Boston, Boston, Massachusetts 02125, United States;* orcid.org/0000-0002-4839-3179; Email: kim.hamad@umb.edu

Authors

Delyan Hristov − *Department of Engineering, University of Massachusetts Boston, Boston, Massachusetts 02125, United States*

Hom Rijal − *Department of Chemistry, University of Massachusetts Boston, Boston, Massachusetts 02125, United States*

Jose Gomez-Marquez − *Little Devices Lab, Massachusetts Institute of Technology, Cambridge, Massachusetts 02139, United States*

Complete contact information is available at: https://pubs.acs.org/10.1021/acs.analchem.0c05438

Author Contributions

D.R.H. designed and carried out the studies and wrote and edited the manuscript, H.R. carried out the studies and wrote and edited the manuscript, J.G.M. wrote and edited the manuscript, and K.H.S. designed the studies and wrote and edited the manuscript.

Funding

This work was supported by UMass Boston.

Notes

The authors declare no competing financial interest.

■ ACKNOWLEDGMENTS

We thank UMass Boston for support during the pandemic and Godwin Ujialele for experimental assistance.

■ ABBREVIATIONS

BSA	bovine serum albumin
DLS	dynamic light scattering
HS	human serum
LOD	limit of detection
NP	nanoparticle
RSD	relative standard deviation

■ REFERENCES

(1) Fu, L.; Wang, B.; Yuan, T.; Chen, X.; Ao, Y.; Fitzpatrick, T.; Li, P.; Zhou, Y.; Lin, Y.; Duan, Q.; Luo, G.; Fan, S.; Lu, Y.; Feng, A.; Zhan, Y.; Liang, B.; Cai, W.; Zhang, L.; Du, X.; Li, L.; Shu, Y.; Zou, H. *J. Infect.* **2020**, *80*, 656−665.

(2) Docherty, A. B.; Harrison, E. M.; Green, C. A.; Hardwick, H. E.; Pius, R.; Norman, L.; Holden, K. A.; Read, J. M.; Dondelinger, F.; Carson, G.; Merson, L.; Lee, J.; Plotkin, D.; Sigfrid, L.; Halpin, S.; Jackson, C.; Gamble, C.; Horby, P. W.; Nguyen-Van-Tam, J. S.; Ho, A.; Russell, C. D.; Dunning, J.; Openshaw, P. J. M.; Baillie, J. K.; Semple, M. G. *BMJ* **2020**, *369*, m1985.
(3) Buitrago-Garcia, D.; Egli-Gany, D.; Counotte, M. J.; Hossmann, S.; Imeri, H.; Ipekci, A. M.; Salanti, G.; Low, N. *PLOS Med.* **2020**, *17*, No. e1003346.
(4) Ing, A. J.; Cocks, C.; Green, J. P. *Thorax* **2020**, *75*, 693−694.
(5) Petersen, I.; Phillips, A. *Clin. Epidemiol.* **2020**, *Volume 12*, 1039−1043.
(6) Wang, J.; Yiu, B.; Obermeyer, J.; Filipe, C. D. M.; Brennan, J. D.; Pelton, R. *Biomacromolecules* **2012**, *13*, 559−564.
(7) Phillips, E. A.; Young, A. K.; Albarran, N.; Butler, J.; Lujan, K.; Hamad-Schifferli, K.; Gomez-Marquez, J. *Adv. Healthcare Mater.* **2018**, 1800104.
(8) Sánchez-Purrà, M.; Roig-Solvas, B.; Rodríguez-Quijada, C.; Leonardo, B.; Hamad-Schifferli, K. *ACS Omega* **2018**, *3*, 10733−10742.
(9) Hristov, D.; Rodríguez-Quijada, C.; Gomez-Marquez, J.; Hamad-Schifferli, K. *Sensors* **2019**, *19*, 554.
(10) Chen, B.; Tian, E.-K.; He, B.; Tian, L.; Han, R.; Wang, S.; Xiang, Q.; Zhang, S.; El Arnaout, T.; Cheng, W. *Signal Transduction Targeted Ther.* **2020**, *5*, 89.
(11) Radzikowska, U.; Ding, M.; Tan, G.; Zhakparov, D.; Peng, Y.; Wawrzyniak, P.; Wang, M.; Li, S.; Morita, H.; Altunbulakli, C.; Reiger, M.; Neumann, A. U.; Lunjani, N.; Traidl-Hoffmann, C.; Nadeau, K. C.; O'Mahony, L.; Akdis, C.; Sokolowska, M. *Allergy* **2020**, *75*, 2829−2844.
(12) Rezaei, M.; Ziai, S. A.; Fakhri, S.; Pouriran, R. *J. Cell. Physiol.* **2020**, *236*, 2430−2442.
(13) Rehman, S. U.; Shafique, L.; Ihsan, A.; Liu, Q. *Pathogens* **2020**, *9*, 240.
(14) Li, Q.; Wu, J.; Nie, J.; Zhang, L.; Hao, H.; Liu, S.; Zhao, C.; Zhang, Q.; Liu, H.; Nie, L.; Qin, H.; Wang, M.; Lu, Q.; Li, X.; Sun, Q.; Liu, J.; Zhang, L.; Li, X.; Huang, W.; Wang, Y. *Cell* **2020**, *182*, 1284−1294.
(15) Azzi, L.; Maurino, V.; Baj, A.; Dani, M.; d'Aiuto, A.; Fasano, M.; Lualdi, M.; Sessa, F.; Alberio, T. *J. Dent. Res.* **2020**, *100*, 115−123.
(16) Hristov, D. R.; Pimentel, A. J.; Ujialele, G.; Hamad-Schifferli, K. *ACS Appl. Mater. Interfaces* **2020**, *12*, 34620−34629.
(17) Schneider, C. A.; Rasband, W. S.; Eliceiri, K. W. *Nat. Methods* **2012**, *9*, 671−675.
(18) Walls, A. C.; Park, Y.-J.; Tortorici, M. A.; Wall, A.; McGuire, A. T.; Veesler, D. *Cell* **2020**, *181*, 281−292.
(19) Tam, J. O.; de Puig, H.; Yen, C.; Bosch, I.; Gómez-Márquez, J.; Clavet, C.; Hamad-Schifferli, K.; Gehrke, L. *J. Immunoassay Immunochem.* **2017**, *38*, 355−377.
(20) Cate, D.; Hsieh, H.; Glukhova, V.; Bishop, J. D.; Hermansky, H. G.; Barrios-Lopez, B.; Grant, B. D.; Anderson, C. E.; Spencer, E.; Kuhn, S.; Gallagher, R.; Rivera, R.; Bennett, C.; Byrnes, S. A.; Connelly, J. T.; Dewan, P. K.; Boyle, D. S.; Weigl, B. H.; Nichols, K. P. Antibody Screening Results for Anti-Nucleocapsid Antibodies Towards the Development of a SARS-CoV-2 Nucleocapsid Protein Antigen Detecting Lateral Flow Assay. *ChemRxiv* **2020**, https://doi.org/10.26434/chemrxiv.12709538.v1.
(21) Rodríguez-Quijada, C.; Gomez-Marquez, J.; Hamad-Schifferli, K. *ACS Nano* **2020**, *14*, 6626−6635.
(22) Kazakov, V. N.; Udod, A. A.; Zinkovych, I. I.; Fainerman, V. B.; Miller, R. *Colloids Surf., B* **2009**, *74*, 457−461.
(23) Baliga, S.; Muglikar, S.; Kale, R. *J. Indian Soc. Periodontol.* **2013**, *17*, 461−465.
(24) Humphrey, S. P.; Williamson, R. T. *J. Prosthet. Dent.* **2001**, *85*, 162−169.
(25) Chen, W.-H.; Hotez, P. J.; Bottazzi, M. E. *Hum. Vaccines Immunother.* **2020**, *16*, 1239−1242.
(26) Wu, Y., Strong evolutionary convergence of receptor-binding protein spike between COVID-19 and SARS-related coronaviruses. *bioRxiv* **2020**, DOI: 10.1101/2020.03.04.975995.
(27) de Puig, H.; Bosch, I.; Carré-Camps, M.; Hamad-Schifferli, K. *Bioconjugate Chem.* **2017**, *28*, 230−238.
(28) Cevik, M.; Kuppalli, K.; Kindrachuk, J.; Peiris, M. *BMJ* **2020**, *371*, m3862.
(29) Owusu, M.; Annan, A.; Corman, V. M.; Larbi, R.; Anti, P.; Drexler, J. F.; Agbenyega, O.; Adu-Sarkodie, Y.; Drosten, C. *PLoS One* **2014**, *9*, No. e99782.
(30) Dijkman, R.; Jebbink, M. F.; Gaunt, E.; Rossen, J. W. A.; Templeton, K. E.; Kuijpers, T. W.; van der Hoek, L. *J. Clin. Virol.* **2012**, *53*, 135−139.
(31) Heimdal, I.; Moe, N.; Krokstad, S.; Christensen, A.; Skanke, L. H.; Nordbø, S. A.; Døllner, H. *J. Infect. Dis.* **2019**, *219*, 1198−1206.
(32) Kim, D.; Quinn, J.; Pinsky, B.; Shah, N. H.; Brown, I. *JAMA* **2020**, *323*, 2085−2086.
(33) Kondo, Y.; Miyazaki, S.; Yamashita, R.; Ikeda, T. *BMJ Case Reports* **2020**, *13*, No. e236812.
(34) Salvati, A.; Pitek, A. S.; Monopoli, M. P.; Prapainop, K.; Bombelli, F. B.; Hristov, D. R.; Kelly, P. M.; Åberg, C.; Mahon, E.; Dawson, K. A. *Nat. Nanotechnol.* **2013**, *8*, 137−143.
(35) Grant, B. D.; Anderson, C. E.; Williford, J. R.; Alonzo, L. F.; Glukhova, V. A.; Boyle, D. S.; Weigl, B. H.; Nichols, K. P. *Anal. Chem.* **2020**, *92*, 11305−11309.
(36) Wölfel, R.; Corman, V. M.; Guggemos, W.; Seilmaier, M.; Zange, S.; Müller, M. A.; Niemeyer, D.; Jones, T. C.; Vollmar, P.; Rothe, C.; Hoelscher, M.; Bleicker, T.; Brünink, S.; Schneider, J.; Ehmann, R.; Zwirglmaier, K.; Drosten, C.; Wendtner, C. *Nature* **2020**, *581*, 465−469.
(37) Bar-On, Y. M.; Flamholz, A.; Phillips, R.; Milo, R. *eLife* **2020**, *9*, No. e57309.
(38) Wang, Y.; Zhang, L.; Sang, L.; Ye, F.; Ruan, S.; Zhong, B.; Song, T.; Alshukairi, A. N.; Chen, R.; Zhang, Z.; Gan, M.; Zhu, A.; Huang, Y.; Luo, L.; Mok, C. K. P.; Al Gethamy, M. M.; Tan, H.; Li, Z.; Huang, X.; Li, F.; Sun, J.; Zhang, Y.; Wen, L.; Li, Y.; Chen, Z.; Zhuang, Z.; Zhuo, J.; Chen, C.; Kuang, L.; Wang, J.; Lv, H.; Jiang, Y.; Li, M.; Lin, Y.; Deng, Y.; Tang, L.; Liang, J.; Huang, J.; Perlman, S.; Zhong, N.; Zhao, J.; Malik Peiris, J. S.; Li, Y.; Zhao, J. *J. Clin. Invest.* **2020**, 5235−5244.
(39) Pan, Y.; Zhang, D.; Yang, P.; Poon, L. L. M.; Wang, Q. *Lancet Infect. Dis.* **2020**, *20*, 411−412.
(40) Weissleder, R.; Lee, H.; Ko, J.; Pittet, M. J. *Sci. Transl. Med.* **2020**, *12*, eabc1931.
(41) Russo, L.; Sánchez-Purrà, M.; Rodríguez-Quijada, C.; Leonardo, B. M.; Puntes, V.; Hamad-Schifferli, K. *Nanoscale* **2019**, *11*, 10819−10827.
(42) Sánchez-Purrà, M.; Carré Camps, M.; de Puig Guixé, H.; Bosch, I.; Gehrke, L.; Hamad-Schifferli, K. *ACS Infect. Dis.* **2017**, *3*, 767−776.
(43) Moghadam, B. Y.; Connelly, K. T.; Posner, J. D. *Anal. Chem.* **2015**, *87*, 1009−1017.
(44) Qin, Z.; Chan, W. C. W.; Boulware, D. R.; Akkin, T.; Butler, E. K.; Bischof, J. C. *Angew. Chem., Int. Ed.* **2012**, *51*, 4358−4361.
(45) Vashist, S. K.; Luppa, P. B.; Yeo, L. Y.; Ozcan, A.; Luong, J. H. T. *Trends Biotechnol.* **2015**, *33*, 692−705.
(46) Gomez-Marquez, J.; Hamad-Schifferli, K. *Nat. Nanotechnol.* **2021**, 484−486.